remote sensing

MDPI

Article

Unmanned Aerial Vehicle (UAV)-Based Vegetation Restoration Monitoring in Coal Waste Dumps after Reclamation

He Ren [1,2], Yanling Zhao [2], Wu Xiao [3,*] and Lifan Zhang [2]

[1] Academy of Eco-Civilization Development for Jing-Jin-Ji Megalopolis, Tianjin Normal University, Tianjin 300387, China; renhe9563@tjnu.edu.cn
[2] Institute of Land Reclamation and Ecological Rehabilitation, China University of Mining and Technology, Beijing 100083, China; ylzhao@cumtb.edu.cn (Y.Z.); bqt2300204058@student.cumtb.edu.cn (L.Z.)
[3] School of Public Affairs, Zhejiang University, Hangzhou 310058, China
* Correspondence: xiaowu@zju.edu.cn; Tel.: +86-13911558318

Abstract: Frequent spontaneous combustion activities restrict ecological restoration of coal waste dumps after reclamation. Effective monitoring of vegetation restoration is important for ensuring land reclamation success and preserving the ecological environment in mining areas. Development of unmanned aerial vehicle (UAV) technology has enabled fine-scale vegetation monitoring. In this study, we focused on *Medicago sativa* L. (alfalfa), a representative herbaceous vegetation type, in a coal waste dump after reclamation in Shanxi province, China. The alfalfa aboveground biomass (AGB) was used as an indicator for assessing vegetation restoration. The objective of this study was to evaluate the capacity of UAV-based fusion of RGB, multispectral, and thermal infrared information for estimating alfalfa AGB using various regression models, including random forest regression (RFR), gradient boosting decision tree (GBDT), K-nearest neighbor (KNN), support vector regression (SVR), and stacking models. The main results are as follows: (i) UAV multi-source data fusion improved alfalfa AGB estimation accuracy, although the enhancement diminished with the increasing number of sensor types. (ii) The stacking model consistently outperformed RFR, GBDT, KNN, and SVR regression models across all feature fusion combinations. It achieved high accuracy with R^2 of 0.86–0.88, RMSE of 80.06–86.87 g/m^2, and MAE of 60.24–62.69 g/m^2. Notably, the stacking model based on only RGB imagery features mitigated the accuracy loss from limited types of features, potentially reducing equipment costs. This study demonstrated the potential of UAV in improving vegetation restoration management of coal waste dumps after reclamation.

Keywords: coal waste dump; vegetation restoration; management strategy; unmanned aerial vehicle; alfalfa aboveground biomass

Citation: Ren, H.; Zhao, Y.; Xiao, W.; Zhang, L. Unmanned Aerial Vehicle (UAV)-Based Vegetation Restoration Monitoring in Coal Waste Dumps after Reclamation. *Remote Sens.* **2024**, *16*, 881. https://doi.org/10.3390/rs16050881

Academic Editors: Giuseppe Modica and Clement Atzberger

Received: 14 January 2024
Revised: 20 February 2024
Accepted: 28 February 2024
Published: 2 March 2024

1. Introduction

Coal mining brings huge economic benefits, while it is also accompanied by many environmental problems [1]. As a primary waste material produced during coal washing and mining, coal gangue typically accounts for 10–15% of coal mining [2]. Due to inadequate planning and implementation, coal gangue is usually artificially piled near the mining areas, forming mountain structures known as coal waste dumps or coal gangue hills [3].

Coal waste dumps occupy vast land resources, causing numerous ecological and environmental problems [4,5]. Effective treatment of coal waste dumps has become a critical environmental protection issue in mining areas. For example, the government of China currently prohibits new coal mines from developing permanent coal waste dumps. Further, ecological protection work such as land reclamation and vegetation restoration were usually carried out for historical coal waste dumps [6]. Depending on the desired restoration outcome (agriculture, forestry, landscape reclamation, etc.), mining enterprises implement land reclamation activities to mitigate the environmental impact of coal waste dumps.

Driven by improved regulations and supportive policies, the ecological restoration of coal waste dumps in China has achieved significant success, with most mining areas exceeding 80% reclamation rates. Coal gangue contains different calorific carbon, residual coal, pyrite, and other flammable substances. It is easy to react in low-temperature oxidation processes and releases a lot of heat when exposed to air and water, leading to spontaneous combustion of coal waste dumps [7,8]. The risk of spontaneous combustion remains even after land reclamation [6,9,10]. Severe and extensive combustion events can destroy the soil environment, leading to vegetation degradation and death [11]. Additionally, local temperature variations may impact vegetation diversity and spatial patterns, hindering ecological restoration of coal waste dumps [12,13]. Therefore, it is crucial to carry out regular monitoring to prevent spontaneous combustion damage to vegetation growth and ensure the ecological restoration in coal waste dumps.

Aboveground biomass (AGB) serves as a critical indicator of vegetation growth and health, and is related to nutritional status, yield, and carbon storage capacity [14]. Coal waste dumps after reclamation are primally composed of herbaceous and shrub vegetation, with some tree plantings in areas with deeper topsoil. Compared to trees and shrubs, herbaceous vegetation exhibits a shorter growth cycle, making it more sensitive to changes in soil environment. Additionally, its extensive coverage renders herbaceous vegetation an effective indicator for evaluating the overall vegetation restoration status of coal waste dumps after reclamation. Traditional field surveys for vegetation AGB are destructive, time-consuming, and labor-intensive. With the rapid advancement of remote sensing technology, AGB monitoring of different vegetation types (e.g., grass, forest, mangrove) based on various satellite remote sensing data has been realized at global, national, or regional scales [15–17]. Due to the advantages of high temporal resolution and large coverage, satellite remote sensing is widely used for continuous monitoring of vegetation change. However, it is still limited by coarse resolution in fine monitoring at the field scale. In recent years, unmanned aerial vehicles (UAVs) have developed rapidly in various application fields [18]. Equipped with different types of sensors, UAVs can quickly capture centimeter-level remote sensing images of research objects in real time, which has become a common method for crop AGB monitoring, such as barley [19], potato [20], wheat [14,21,22], etc.

Spectral, structural, thermal, and texture information extracted from UAV data has been widely used for crop growth monitoring. Through traditional regression models (e.g., linear regression, partial least squares regression), or machine learning regression models (e.g., random forest, artificial neutral networks, support vector regression), crop traits can be linked to UAV imagery features. For example, canopy structure information derived from UAV-based RGB imagery was employed for alfalfa plant height estimation [10], as well as maize chlorophyll [23] and winter wheat yield [24] estimation from UAV spectral information. Recent studies demonstrated that the combination of different UAV imagery features can significantly improve estimation accuracy. Yue et al. [14] found that incorporating height information can improve the estimation accuracy of winter wheat AGB. The R^2 of their estimation model increased by more than 0.2, and RMSE decreased more than 0.6 t/ha. Liu et al. [20] indicated that crop height may contribute to potato AGB estimation. Moreover, the combination of canopy thermal information with spectral and structural information has been shown to improve the stability of crop yield estimation, such as wheat [21] and soybean [25]. While the fusion of multi-source UAV remote sensing data provides great potential for crop growth monitoring, it undoubtedly increases the cost. At present, the application of UAV-based vegetation restoration monitoring is still limited by cost and operational constraints [18]. In addition to the estimation accuracy, cost is also a major concern for mining enterprises. Therefore, it is essential to propose a feasible UAV-based vegetation restoration monitoring strategy of coal waste dumps.

To address this issue, an investigation was conducted at a typical reclaimed coal waste dump in Shanxi Province, China. Taking the artificially planted vegetation type in the study area, *Medicago sativa L.* (alfalfa), as the research object, this study achieved the monitoring of vegetation restoration in a coal waste dump, with the support of UAV multi-source remote

sensing imagery (RGB, multispectral, and thermal infrared) and field surveys. The primary objectives of this study were as follows: (i) to determine whether UAV multi-source data fusion can significantly improve the estimation accuracy of alfalfa AGB, and (ii) to evaluate the performance of various regression models. Our study aimed to propose an improved UAV-based strategy for accurate estimation of alfalfa AGB in coal waste dumps.

2. Materials and Methods

2.1. Study Area

The study area was located in Wangzhuang coal mine, Changzhi city, Shanxi province (113°1′–113°9′E, 35°55′–36°22′N). Shanxi province, a major coal producer in China, contributed 1.3 billion tons in 2022, nearly 1/3 of the national output. This extensive mining activity generated over 1.7 billion tons of coal gangue, resulting in thousands of coal waste dumps. Notably, 619 of 1477 coal waste dumps (42%) in Shanxi province have either burned or are currently burning, posing significant environmental threats [26].

Land reclamation and ecological restoration were carried out at the selected coal waste dump in 2014. A spiral structure with a top platform and three-layer slopes was formed through terrain leveling (Figure 1). The height of the dump was approximately 36 m, with slopes ranging from 32° to 35° and covering 3.9 hectares. To facilitate greening and minimize soil erosion, a 0.5–1 m thick loess layer was applied, followed by planting local pioneer vegetation species. The dominant vegetation species were *Platycladus orientalis*, *Amorpha fruticosa* L., *Medicago sativa* L., and *Rhus typhina*. The vegetation restoration proved successful, with no observed spontaneous combustion of the coal waste dump.

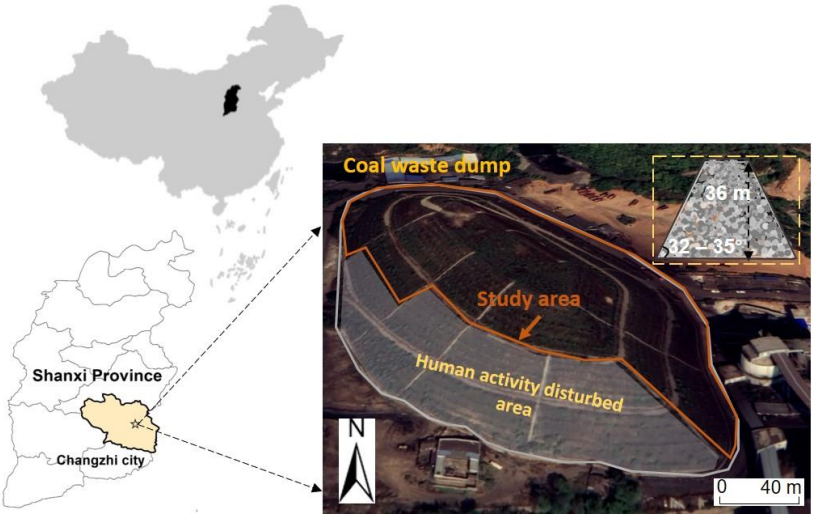

Figure 1. Location of the study area.

However, a field survey in October 2020 revealed significant degradation of vegetation on the northeastern and southeastern slopes. There were signs of burning on surface vegetation in some regions, and the surface soil was exposed [6]. Consequently, it was necessary to carry out vegetation restoration monitoring in the study area. Since the vegetation on the south side of the coal waste dump was disturbed by human activity during the field survey, this region was excluded during the survey (Figure 1).

2.2. Data Source

2.2.1. UAV Data Collection and Preprocessing

A Matrice210 UAV (DJI Tech., Shenzhen, China) equipped with a ZenmuseX5S camera (DJI Tech., Shenzhen, China), a Micasence Rededge MX camera (Micasence, Seattle, WA, USA), and a ZenmuseXT2 camera (DJI Tech., Shenzhen, China) was used to capture the red–green–blue (RGB) image, multispectral reflectance, and temperature data, respectively. Data collection occurred under cloudless weather conditions between 11:00 and 12:30 h,

with a flight of 80 m, ensuring complete coverage of the coal waste dump. RGB and multispectral images were acquired simultaneously, and the photograph forward and lateral overlaps were 80% and 70%, respectively. Thermal infrared images were subsequently captured with 85% and 80% forward and lateral overlap, respectively. To achieve accurate georeferencing, the flight mission was carried out in RTK mode based on the geographic coordinate system of the mining area (Beijing 54 3°, where the central meridian is 114°E). The Pix4Dmapper4.4.12 software (Pix4D SA) was used to process and generate the UAV products in this study. The average ground sample distance (GSD) of RGB imagery, multispectral reflectance, and thermal imagery was 2.26 cm, 7.40 cm, and 8.98 cm/pixel, respectively. The details on data acquisition and processing methods can be found in our previous research [10].

2.2.2. Alfalfa AGB Measurement

Herbaceous vegetation covers a wide area and responds sensitively to soil environmental changes due to its shorter growth cycle. Therefore, the representative herbaceous species *Medicago sativa* L. (alfalfa) was selected in this study. Alfalfa AGB sampling points were systematically distributed across the coal waste dump. However, noticeable signs of spontaneous combustion and variations in alfalfa growth were observed on the northwest and southeast slopes (regions I and II) during the field survey. Consequently, we allocated more sample points to Regions I and II to ensure a representative sample of alfalfa AGB values.

There were 29 and 44 alfalfa sampling points in regions I and II, respectively, with an additional 87 points in other areas, for a total of 160 sampling points (Figure 2). To minimize the influence of spatial heterogeneity, the quadrat method was employed with 20 cm × 20 cm quadrats at each point. Considering the potential impact of traditional grassland survey methods, five random alfalfa samples were collected within each quadrat to minimize secondary damage. These samples were stored in pre-weighed PE plastic bags and weighed using a balance accurate to 0.01 g. Additionally, the number of individual plants (n) and average height (h) within each quadrat were recorded, with the main stem serving as the statistical unit. The alfalfa AGB for each sampling point was then calculated using Equation (1):

$$AGB(g/m^2) = \frac{1}{0.04} n \times m_1 \quad (1)$$

where n is the number of alfalfa plants recorded in each sampling point, and m_1 is the average weight of five measured alfalfa plants.

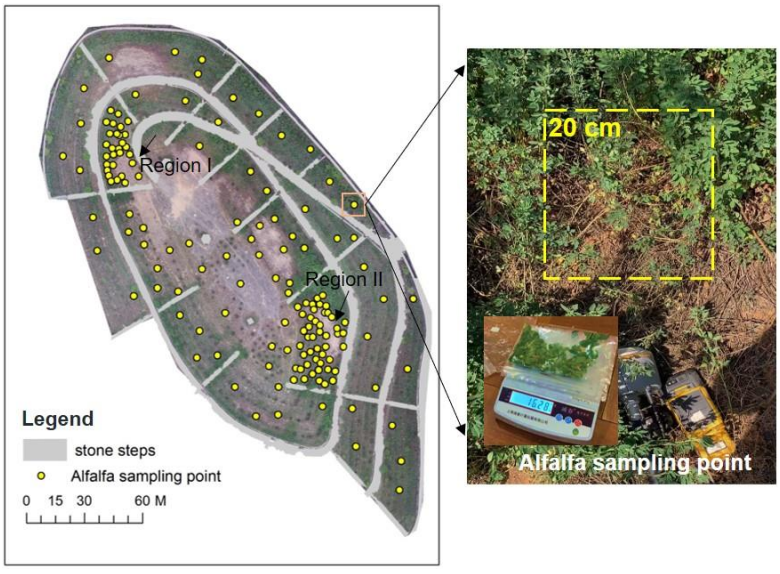

Figure 2. Alfalfa aboveground biomass (AGB) measurement in the study area.

3. Methodology

3.1. Alfalfa Coverage Extraction

Alfalfa coverage in the coal waste dump was extracted based on the UAV RGB imagery using the object-based image analysis (OBIA) method. Further details on the process can be found in Supplementary Material.

3.2. UAV Imagery Feature Extraction

3.2.1. Spectral Information

A set of vegetation indices (VIs) derived from RGB and multispectral sensors, previously used for vegetation AGB estimation, were chosen to estimate the alfalfa AGB in this study (Table 1).

Table 1. UAV imagery features extraction in this study.

Imagery Feature	Sensor	Imagery Feature	Calculation	Reference
Spectral information	RGB	Normalized Green–Red Difference Index (NGRDI)	NGRDI = (G − R)/(G + R)	[27]
	RGB	Color Index of Vegetation Extraction (CIVE)	CIVE = 0.441r − 0.881g + 0.385b + 18.78745	[28]
	RGB	Excess Green Index (EXG)	EXG = 2g − r − b	[29]
	RGB	Excess Green Minus Excess Red Index (EXGR)	EXGR = EXG − 1.4r − g	[30]
	RGB	Modified Green–Red Vegetation Index (MGRVI)	MGRVI = $(g^2 - r^2)/(g^2 + r^2)$	[19]
	RGB	RGB-based Vegetation Index (RGBVI)	RGBVI = $(g^2 - rb)/(g^2 + rb)$	[31]
	RGB	Visible Atmospherically Resistant Index (VARI)	VARI = (g − r)/(g + r − b)	[28]
	RGB	Green Leaf Index (GLI)	GLI = (2g − r − b)/(2g + r + b)	[31]
	RGB	Green–Red Vegetation Index (GRVI)	GRVI = (g − r)/(g + r)	[19]
	RGB	Normalized Green–Blue Difference Vegetation Index (NGBDI)	NGBDI = (g − b)/(g + b)	[32]
	MS	Green Normalized Difference Vegetation Index (GNDVI)	(ρNIR − ρGreen)/(ρNIR + ρGreen)	[33]
	MS	Normalized Difference Vegetation Index (NDVI)	(ρNIR − ρRed)/(ρNIR + ρRed)	[34]
	MS	Nonlinear Vegetation Index (NLI)	$(\rho NIR^2 - \rho Red)/(\rho NIR^2 + \rho Red)$	[35]
	MS	Enhanced Vegetation Index (EVI)	2.5(ρNIR − ρRed)/(ρNIR + 6ρRed − 7.5ρBlue + 1)	[36]
	MS	Ratio Vegetation Index (RVI)	ρNIR/ρRed	[37]
	MS	Optimized Soil Adjusted Vegetation Index (OSAVI)	(ρNIR − ρRed)/(ρNIR + ρRed + 0.16)	[38]
	MS	Modified Simple Ratio (MSR)	$(\rho NIR/\rho Red - 1)/(\rho NIR/\rho Red + 1)^{1/2}$	[39]
	MS	Green Chlorophyll Index (CIgreen)	ρNIR/ρGreen − 1	[27]
	MS	Normalized Difference Rededge Index (NDRE)	(ρNIR-ρRededge)/(PNIR+ρRededge)	[40]
	MS	Chlorophyll Index-rededge (CIrededge)	ρNIR/ρRededge − 1	[27]
Texture information	RGB/MS/TIR	MEA, HOM, COR, DIS, ENT, CON, SEC, VAR	GLCM	[41]
Thermal information	TIR	Canopy temperature depression (CTD)	$T_{canopy} - T_{air}$	[42]
	TIR	Crop water stress index (CWSI)	$(T_{canopy} - T_{wet})/(T_{dry} - T_{wet})$	[43]
Structure information	RGB	Plant height (PH)	DSM–DEM	[19]

R, G, and B are the digital number (DN) values of red, green, and blue bands of the RGB sensor, respectively. r, g, and b are the normalized red, green, and blue bands, respectively; r = R/(R + G + B), g = G/(R + G + B), and b = B/(R + G + B). ρRed, ρGreen, ρBlue, ρNIR, and ρRededge are the reflectance of red, green, blue, near infrared, and red edge band of the multispectral sensor, respectively. T_{canopy} is the canopy temperature of alfalfa coverage, and T_{air} represents the mean air temperature (29 °C used in this study). T_{wet} (0.5% of the T_{canopy}) and T_{dry} (99.5% of the T_{canopy}) represent the temperature of fully transpired leaves with open stomata and non-transpired leaves with closed stomata, respectively.

3.2.2. Texture Information

UAV imagery texture features are commonly used for plant AGB estimation. In total, eight texture metrics were incorporated in this study: mean (MEA), homogeneity (HOM), correlation (COR), dissimilarity (DIS), entropy (ENT), contrast (CON), second moment (SEC), and variance (VAR). Texture information for each band (Red, Green, Blue, Near infrared [NIR], Red edge, and Thermal infrared [TIR]) was extracted using ENVI5.3 software (GLCM module). Based on our previous work, we applied a moving direction

averaging four directions (θ = 0, 45, 90, and 135°), a 3 × 3 moving window, and a 1-pixel moving step.

3.2.3. Thermal Information

Canopy temperature is known to enhance estimations of various vegetation growth parameters. In this study, the alfalfa plants exhibited kraurotic and hydroponic characteristics under spontaneous combustion processes. Accordingly, temperature information offered valuable additional information for alfalfa AGB estimation. For this purpose, two TIR imagery features, namely canopy temperature depression (CTD) and statistical crop water stress index (CWSIs), were selected in this study (Table 1).

3.2.4. Structure Information

Plant height (PH) exhibited a strong correlation with crop AGB, making it a suitable structural characteristic for estimation [14,19]. In this study, the crop height model (CHM) was utilized to extract the alfalfa PH (Table 1). A digital surface model (DSM) was generated from UAV-RGB imagery using Pix4Dmapper4.4.12 software, while a digital elevation model (DEM) was provided by the mining enterprise. The DEM included high-precision terrain data after terrain leveling in the reclamation project, which was measured using a total station. Additionally, a GNSS–real time kinematic (RTK) field survey was performed to ensure the suitability of DEM for estimating alfalfa PH.

3.2.5. Feature Selection

An initial set of 41 UAV RGB imagery features, 50 MS imagery features, and 10 TIR imagery features were extracted. However, to avoid potential negative impacts of excessive features on model performance and efficiency, the Boruta algorithm was employed for feature selection. The Boruta algorithm, developed based on the random forest algorithm [44], has been widely used in crop growth monitoring [24,45]. It operates in several main steps: (a) Shuffling the feature values of each feature matrix X, and then forming a new feature matrix combined with real features and shadow features. (b) Using the new feature matrix as input to obtain the model of feature importance after training. (c) Calculating the Z_score of real and shadow features and recording the largest Z_score as Zmax. A Z_score greater than Zmax is marked as "important", and a Z_score significantly less than Zmax is marked as "unimportant". "Unimportant" factors are removed from the feature dataset. (d) Steps (a)–(c) are repeated until all features are marked.

Following this process, a final set of eight RGB features, eight MS features, and three TIR features were obtained for further analysis (Table 2).

Table 2. Feature selection results based on the Boruta algorithm.

Sensor Type	Select Feature	Number
RGB	PH, EXGR, CIVE, VARI, NGRDI, MGRVI, GRVI, and G_VAR	8
MS	RVI, NDRE, OSAVI, NDVI, MSR, CI-rededge, R_MEA, and NIR_MEA	8
TIR	CWSIs, thermal_VAR, and thermal_MEA	3

3.3. Modeling Method

Commonly used machine learning models, random forest regression (RFR), support vector regression (SVR), gradient boosting decision tree (GBDT), and K-nearest neighbor (KNN) were employed for alfalfa AGB estimation. Additionally, a stacking algorithm was implemented to improve estimation accuracy by combining these individual models.

The stacking algorithm operates by training a series of independent base models in parallel and then using a meta model to combine their predictions [46]. As shown in Figure 3, the stacking model mainly consisted of three parts in this study: (a) The train data was divided to k datasets using k-fold cross-validation (k = 5 in this study) firstly, and each

base model (RFR, SVR, GBDT, KNN) was then trained on k − 1 datasets. (b) The trained base models were used to predict another dataset and test data, respectively, to obtain the estimation results of the k training datasets and test data. (c) The meta model was trained and then estimated the alfalfa AGB. The estimation results of k training data were used as the training dataset of the meta model, and the average value of the estimation results of k test data was the test dataset. In this study, the meta model was the best-performing model (RFR) among the base-models.

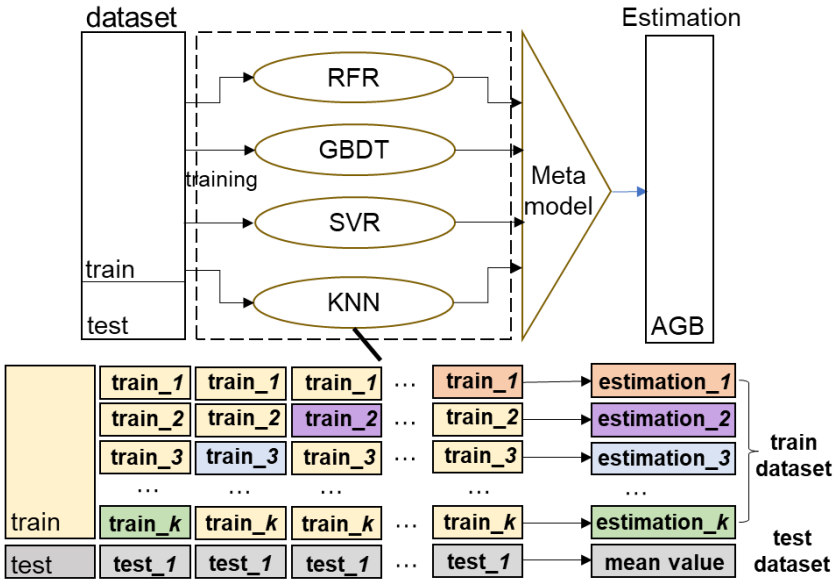

Figure 3. Diagram of stacking model in this study.

3.4. Accuracy Assessment

The performance of the estimation model was evaluated using the coefficient of determination (R^2), root mean square error (RMSE), and mean absolute error (MAE). The R^2 ranges from −1 to 1, with higher values indicating a stronger correlation between estimated and measured values. Lower RMSE and MAE values reflect better estimation accuracy. The calculations of these metrics are provided in Equations (2)–(4):

$$R^2 = 1 - \frac{\sum_{i=1}^{N}(y_i - \hat{y}_i)^2}{\sum_{i=1}^{N}(y_i - \overline{y}_i)^2} \quad (2)$$

$$RMSE = \sqrt{\frac{1}{N}\sum_{i=1}^{N}(y_i - \hat{y}_i)^2} \quad (3)$$

$$MAE = \frac{1}{N}\sum_{i=1}^{N}\left|y_i - \hat{y}_i\right| \quad (4)$$

where, N (i = 1, 2, 3, . . ., N) represents the number of alfalfa samples, y_i is the measured value of ith alfalfa sample, $\hat{y}_i$ is the estimated value of ith alfalfa sample, and $\overline{y}_i$ is the average value of measured alfalfa samples.

3.5. Workflow in This Study

Given the cost-effectiveness of RGB imagery, it is the most commonly used data type in mining areas [18]. To this end, this study investigated four combinations, Combination I (RGB), Combination II (RGB + MS), Combination III (RGB + TIR), and Combination IV (RGB + MS + TIR), to explore the impact of UAV imagery feature fusion on alfalfa AGB

estimation accuracy. The estimation performances of different machine learning models (RFR, GBDT, SVR, KNN, and stacking) were also compared. The workflow of this study is illustrated in Figure 4.

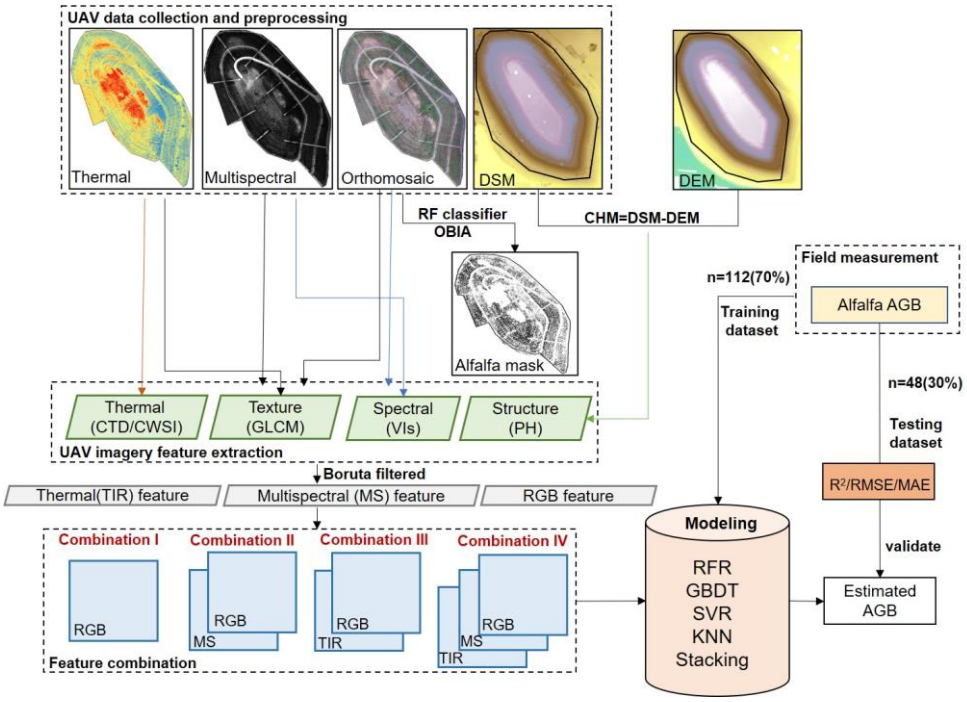

Figure 4. Research flowchart in this study.

4. Results and Discussion

4.1. Modeling and Validation of Alfalfa AGB

The alfalfa AGB estimation results are presented in Table 3 and Figure 5. It was observed that a better estimation of alfalfa AGB can be achieved based on RGB imagery features (Combination I). The R^2 of each model in the test dataset was in the range 0.62–0.86, with RMSE ranging from 86.6 g/m^2 to 143.94 g/m^2, and MAE ranging from 60.24 g/m^2 to 92.83 g/m^2.

Table 3. Alfalfa AGB estimation results under feature combinations.

Model	Metric	Combination I		Combination II		Combination III		Combination IV	
		Train	Test	Train	Test	Train	Test	Train	Test
RFR	R^2	0.96	0.82	0.96	0.87	0.96	0.86	0.96	0.87
	RMSE	48.33	96.64	48.51	84.87	48.65	85.97	48.17	84.36
	MAE	34.73	68.28	35.05	65.21	33.38	59.02	33.53	61.56
SVR	R^2	0.77	0.62	0.85	0.76	0.85	0.77	0.85	0.77
	RMSE	115.62	143.94	94.80	113.19	93.21	111.30	92.78	110.97
	MAE	77.68	92.83	55.30	76.60	52.50	73.78	52.04	73.45
GBDT	R^2	0.85	0.78	0.89	0.81	0.85	0.82	0.96	0.83
	RMSE	94.23	107.79	80.08	100.88	93.68	99.16	51.08	96.06
	MAE	72.58	81.62	61.48	79.16	71.83	74.85	39.44	78.64
KNN	R^2	0.77	0.65	0.76	0.79	0.77	0.79	0.79	0.79
	RMSE	114.84	136.53	118.68	107.29	116.75	106.79	107.46	105.58
	MAE	79.68	84.04	82.47	70.51	83.13	72.41	72.70	72.22
Stacking	R^2	0.90	0.86	0.94	0.88	0.93	0.86	0.95	0.88
	RMSE	76.61	86.87	60.31	80.82	62.64	85.34	54.89	80.06
	MAE	55.09	60.24	42.72	61.45	43.79	62.69	37.78	60.31

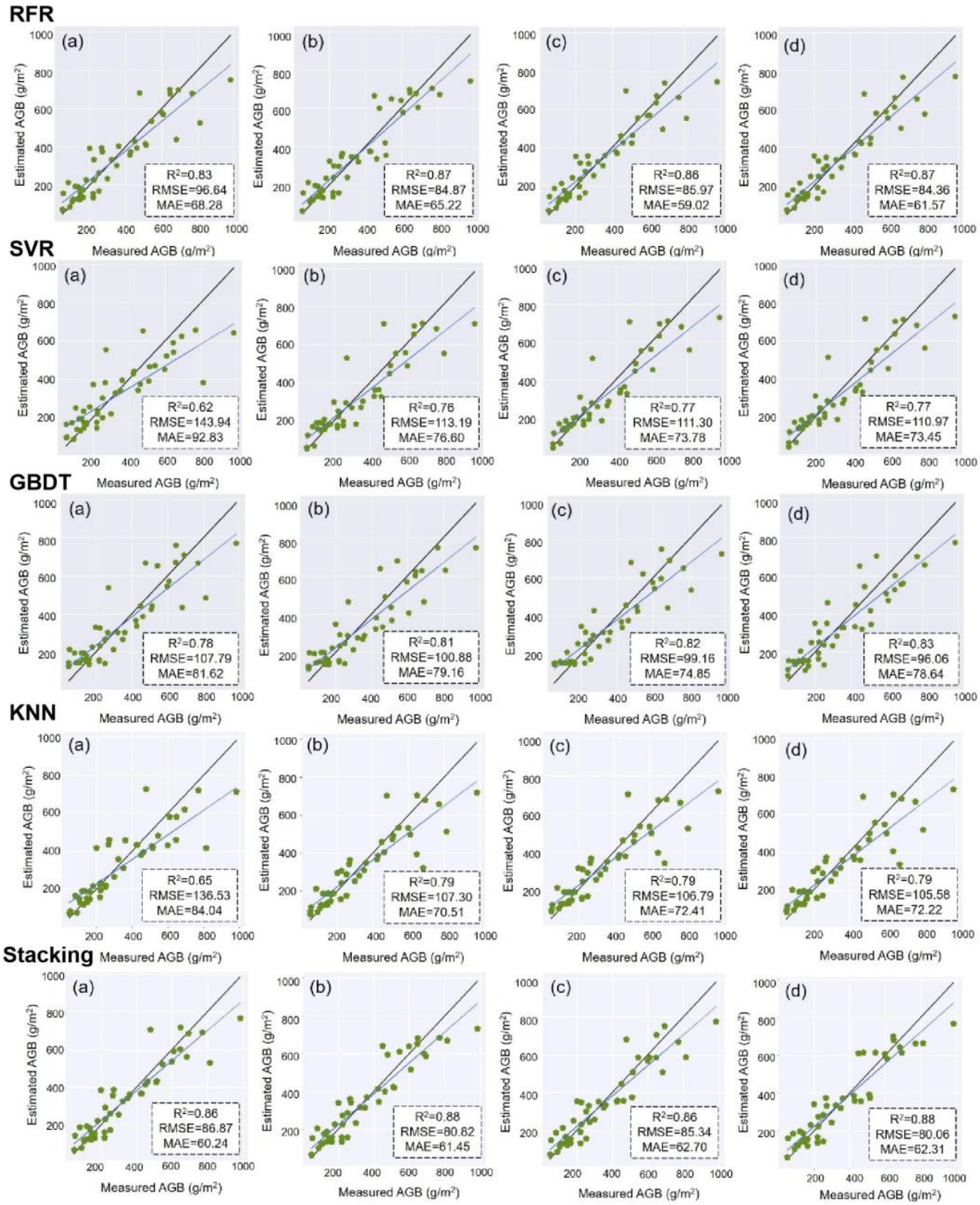

Figure 5. Estimation results of alfalfa AGB based on the random forest regression (RFR), support vector regression (SVR), gradient boosting decision tree (GBDT), K-nearest neighbor (KNN), and stacking model. The green line is the fitted line between the estimated and measured AGB, and the black line indicates a 1:1 relationship. For each model, (**a**) Combination I (RGB); (**b**) Combination II (RGB + MS); (**c**) Combination III (RGB + TIR); (**d**) Combination IV (RGB + MS + TIR).

It was demonstrated that the potential of fusing RGB spectral information, texture information, and structure information for alfalfa AGB estimation, which was consistent with previous studies that have shown the combination of RGB spectral and texture information, can improve the estimation accuracy of crop AGB [6,33]. Furthermore, incorporating crop height into estimation models based on RGB VIs or texture features has also been proven to have great potential in improving the AGB estimation accuracy of potato [20], maize [19], wheat [47], and other crops. The structure information includes the differences in alfalfa canopy and structural features caused by spontaneous combustion, and overcomes the asymptotic saturation issue of spectral features to a certain extent.

4.1.1. Combination of Different Sensors/Information in Alfalfa AGB Estimation

The estimation accuracy of all models improved with the increase in sensor/feature types (Table 3). Compared to Combination I, the estimation performance of all models based on Combinations II and III improved. The R^2 increased by 0.02 to 0.15, while RMSE and MAE decreased by 1.53–32.64 g/m^2 and −2.47–19.05 g/m^2, respectively.

It was observed that the estimation accuracy of alfalfa AGB improved when fusing RGB and MS information (Table 3). Especially for samples that exceeded 400 g/m^2, the estimation model incorporating MS information exhibited superior performance. The reflectance of vegetation varies across different wavebands. Compared to the visible band, the NIR and Red edge band exhibit greater sensitivity to the canopy structure and absorption of chlorophyll, and enhance the vegetation vigor contrast [47–49], thereby improving the estimation accuracy of alfalfa AGB. Canopy temperature is often associated with vegetation leaf water content and canopy structure. Canopy temperature information in this study was derived from UAV TIR data. Although it may be affected by the sensor itself and a wide range of environmental factors, the thermal information also showed great potential for alfalfa AGB estimation. Specifically, compared to using only a single RGB sensor, the fusion of RGB and TIR information (Combination III) substantially improved the estimation accuracy of alfalfa AGB (Table 3). Under the influence of spontaneous combustion of coal waste dump, the alfalfa plants suffered from water shortage and appeared dry. Similar to our research results, Maimaitijiang et al. [25] and Wu et al. [50] pointed out that the introduction of thermal information improved the estimation accuracy of soybean yield and wheat LAI, respectively. Also, Wang et al. [51] reported that TIR features indirectly reflect the difference between the water content of sugar beet root and the surrounding environment, further improving the estimation accuracy of sugar content.

However, the improvement of estimation accuracy was not obvious when three imagery features were further fused (Combination IV). The R^2 of all regression models was basically unchanged (~0–0.02), and RMSE and MAE decreased by 0.5–5.28 g/m^2 and 0.48–3.15 g/m^2. Maimaitijiang et al. [25] suggested that the accuracy improvement in soybean yield was not substantial when combining spectral, structure, thermal, and texture information in comparison with only using multi-sensor-based texture information. Also, Wu et al. [50] found no significant improvement in estimation accuracy of wheat LAI when adding thermal features to spectral and structural features. We believe that this may be due to the information homogeneity and redundancy among features derived from different sensors [52].

4.1.2. Regression Model in Alfalfa AGB Estimation

Machine learning algorithms have great potential in crop growth-parameter estimation. Compared with traditional algorithms, machine learning regression models can obtain higher estimation accuracy when dealing with high-dimensional complex data [50]. The RFR and GBDT models performed better than the SVR and KNN algorithms, which was consistent with previous studies [47,50]. The RFR model based on the fusion of RGB and TIR (Combination III) showed a higher R^2 and lower MAE among all regression models. RFR and GBDT used decision tree-based ensemble learning methods, which can reduce the impact of noise by aggregating multiple decision trees [47]. The SVR model performed

poorly in this study, which may be related to the number (n = 160) and quality of the alfalfa samples.

The stacking model achieved superior performance compared to other regression models under all feature combinations, showing higher R^2 and lower RMSE and MAE values. When using the stacking model based on the fusion of three feature types, the optimal AGB estimation results were observed (Table 3). The R^2 of the model was 0.86, and the RMSE and MAE were 80.06 g/m^2 and 60.31 g/m^2, respectively. Especially for the alfalfa samples with high values (>600 g/m^2), the stacking model showed higher stability (Figure 5). Feng et al. [53] found that the estimation accuracy of alfalfa yield of the stacking model was better than that of RFR, SVR, and KNN models at high numerical values (>2000 kg/ha). Shu et al. [45] reported that the estimation accuracy of ensemble learning models was higher than those of the basic models in maize growth parameters.

In addition, as shown in Figure 6, the estimation ability of all models was improved to varying degrees with the increase in feature types. The estimation accuracy of basic regression models was relatively inferior based on the single RGB sensor (Combination I), and the accuracy was significantly improved when fusing MS or TIR features. However, compared with other regression models, the stacking model maintained a good estimation accuracy when only using the single RGB sensor, even better than the GBDT, KNN, and SVR models under multi-source feature fusion. The stacking model can combine the advantages of multiple base models, showing greater potential in accuracy and stability. Furthermore, our results showed that the stacking model performed better when the available feature information was limited.

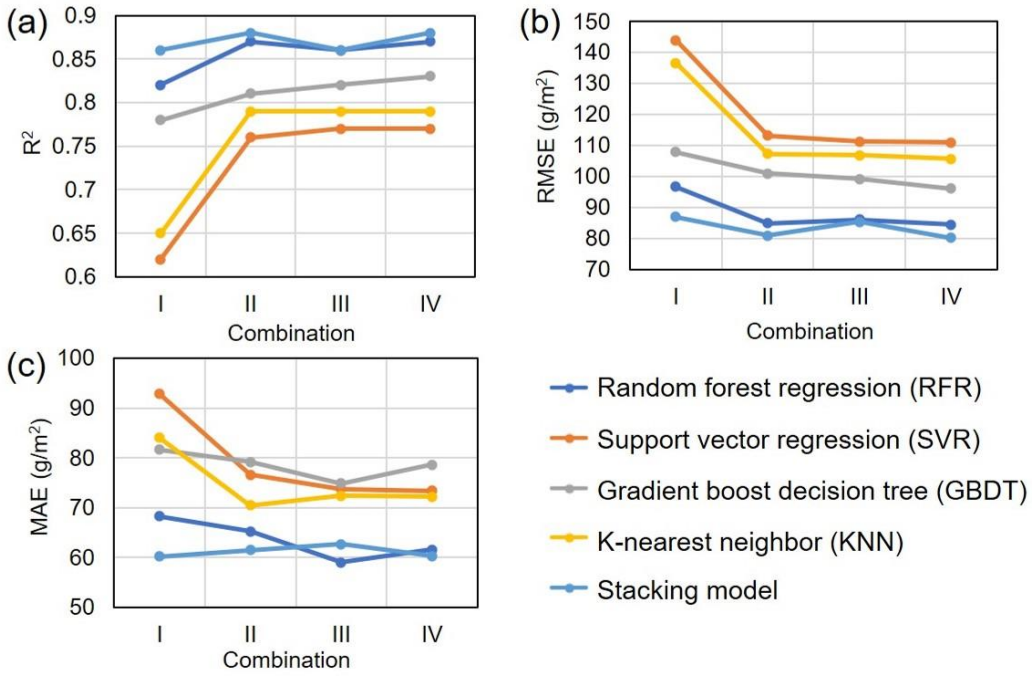

Figure 6. Alfalfa AGB estimation performance of different regression models. (**a**) R^2; (**b**) RMSE; (**c**) MAE.

4.2. Spatial Analysis of Alfalfa AGB in Coal Waste Dump

4.2.1. Map of Alfalfa AGB

The distribution map of Alfalfa AGB in the study area was generated using the optimal model (stacking model and Combination IV) combined with the alfalfa coverage mask, as shown in Figure 7. It was observed that spontaneous combustion caused a substantial impact on vegetation restoration in the study area. Surface alfalfa cover in local regions was damaged due to the spontaneous combustion process, resulting in bare soil areas.

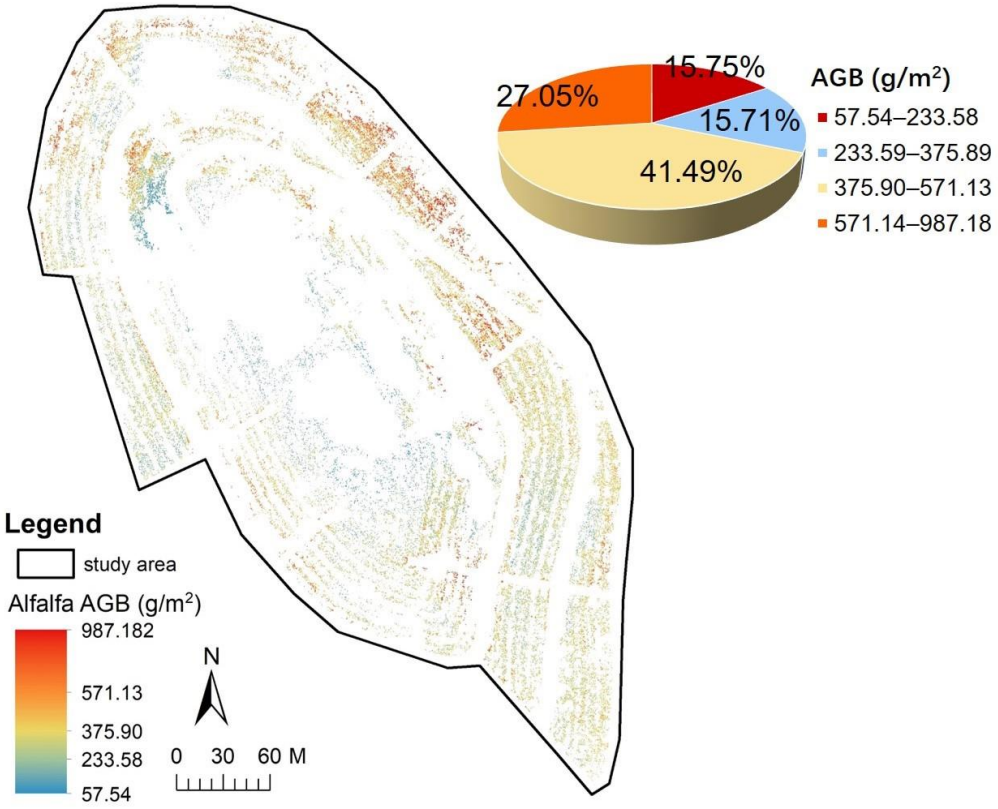

Figure 7. Distribution map of alfalfa aboveground biomass (AGB) in the study area.

The alfalfa AGB was classified into four grades using a natural break method (Figure 7). The proportion of AGB values below 375.89 g/m^2 exceeded 50%, while those above 571.14 g/m^2 constituted only 15.71%. Thus, although the vegetation coverage in the coal waste dump was relatively high, alfalfa growth in local areas exhibited significant spatial variance under the influence of spontaneous combustion.

4.2.2. Alfalfa AGB Response to Spontaneous Combustion of Coal Waste Dump

The alfalfa AGB in some areas exhibited obvious spatial variances under spontaneous combustion. Previous studies indicated that the growth and distribution of surface vegetation can reflect the intensity of underground spontaneous combustion to some extent [6,10,13]. To this end, this study utilized the measured soil temperature (25 cm depth) as a real reference of the intensity of underground spontaneous combustion to explore the response of alfalfa AGB to spontaneous combustion of the coal waste dump. A detailed description of the soil temperature points can be found in Supplementary Material. Considering the measurement scale of soil temperature (1.5 m), the average value of all alfalfa AGB pixels within a 1.5 m buffer zone was calculated. Since some points were located in bare soil areas, the calculated AGB value was set to 0.

Pearson's correlation coefficient revealed a significant negative correlation between alfalfa AGB and soil temperature ($r = -0.639$, $p < 0.01$). Furthermore, a logarithmic relationship was observed between alfalfa AGB and soil temperature ($y = -464.2\ln x + 1857.8$, $R^2 = 0.502$), as shown in Figure 8. Thus, alfalfa AGB can reflect the soil temperature changes caused by underground spontaneous combustion to a certain extent. The intensity of spontaneous combustion was higher in the bare soil areas, resulting in damage to the surface alfalfa coverage under a high-temperature environment. With the weakening of spontaneous combustion, alfalfa was affected by various degrees of temperature, drought, and nutrient deficiency [11], leading to a decrease in AGB values observed in this study (Figure 8). Herbaceous vegetation usually covers a large area, which can reflect the ecological restoration of entire coal waste dumps. Therefore, regular monitoring of vegetation

growth can reveal the underground spontaneous combustion activities to a certain extent, and further reveal the intensity or extent of the spontaneous combustion process through spatial analysis, which is of great significance for the ecological restoration of coal waste dumps after reclamation.

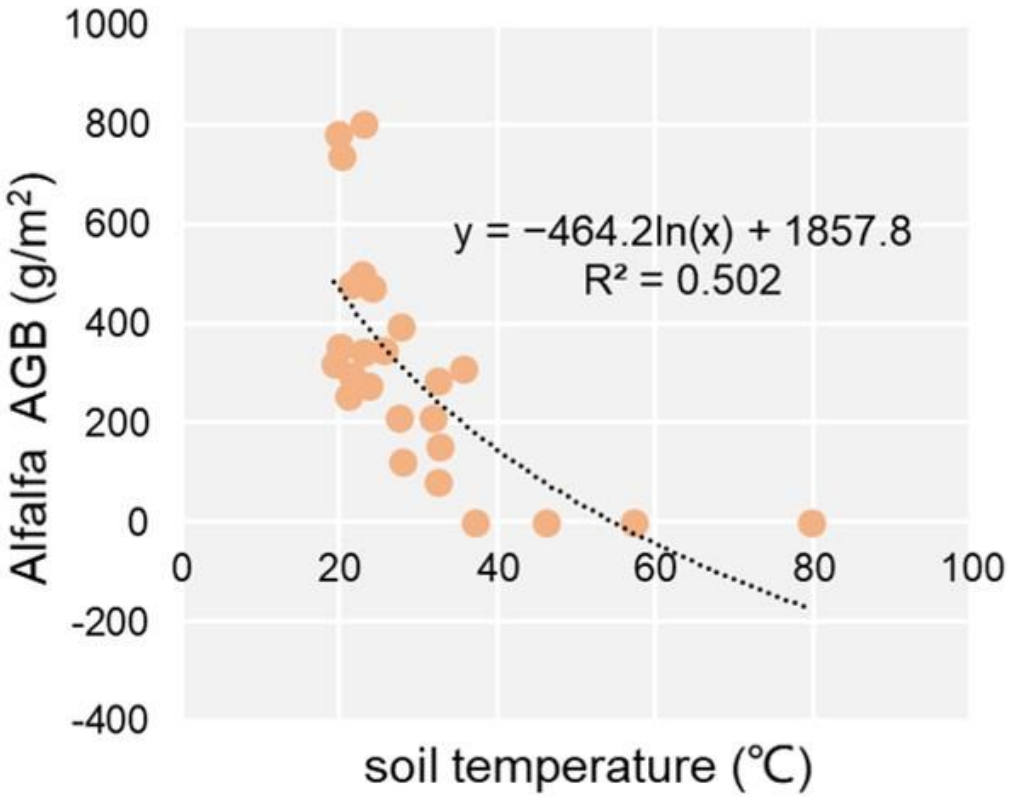

Figure 8. Correlation analysis between soil temperature and alfalfa aboveground biomass (AGB).

4.3. Monitoring Strategy in Vegetation Restoration of Coal Waste Dumps

The above analysis indicates that the stacking model outperformed the other regression models across all feature combinations (Table 3). For three assessment metrics (R^2, RMSE, and MAE), a comparison was performed between the stacking model and other regression models, as shown in Figure 9. The results showed that the R^2 of the stacking model based on the RGB single-sensor remained higher than that of the KNN, SVR, and GBDT models, while being only slightly lower than the RFR model that utilizes multi-sensor data (with an R^2 decrease of 1%). Moreover, the RMSE and MAE of the stacking model were higher than those of the other regression models, except for the RFR model. Despite the relatively complex calculations involved in the stacking model, it effectively compensated for the accuracy loss caused by using only the RGB single-sensor. Additionally, the fusion of three types of sensors contributed to an improvement in the estimation accuracy of the stacking model, but to a lesser extent than the fusion of RGB and MS or TIR data. The R^2 of the fusion of RGB and MS was close to that of the three sensors (0.88). Furthermore, in terms of RMSE and MAE, the Stacking model based on the combination of RGB, MS, and TIR exhibited a decrease of 0.76 g/m^2 and 1.14 g/m^2, respectively, when compared with the fusion of RGB and TIR data.

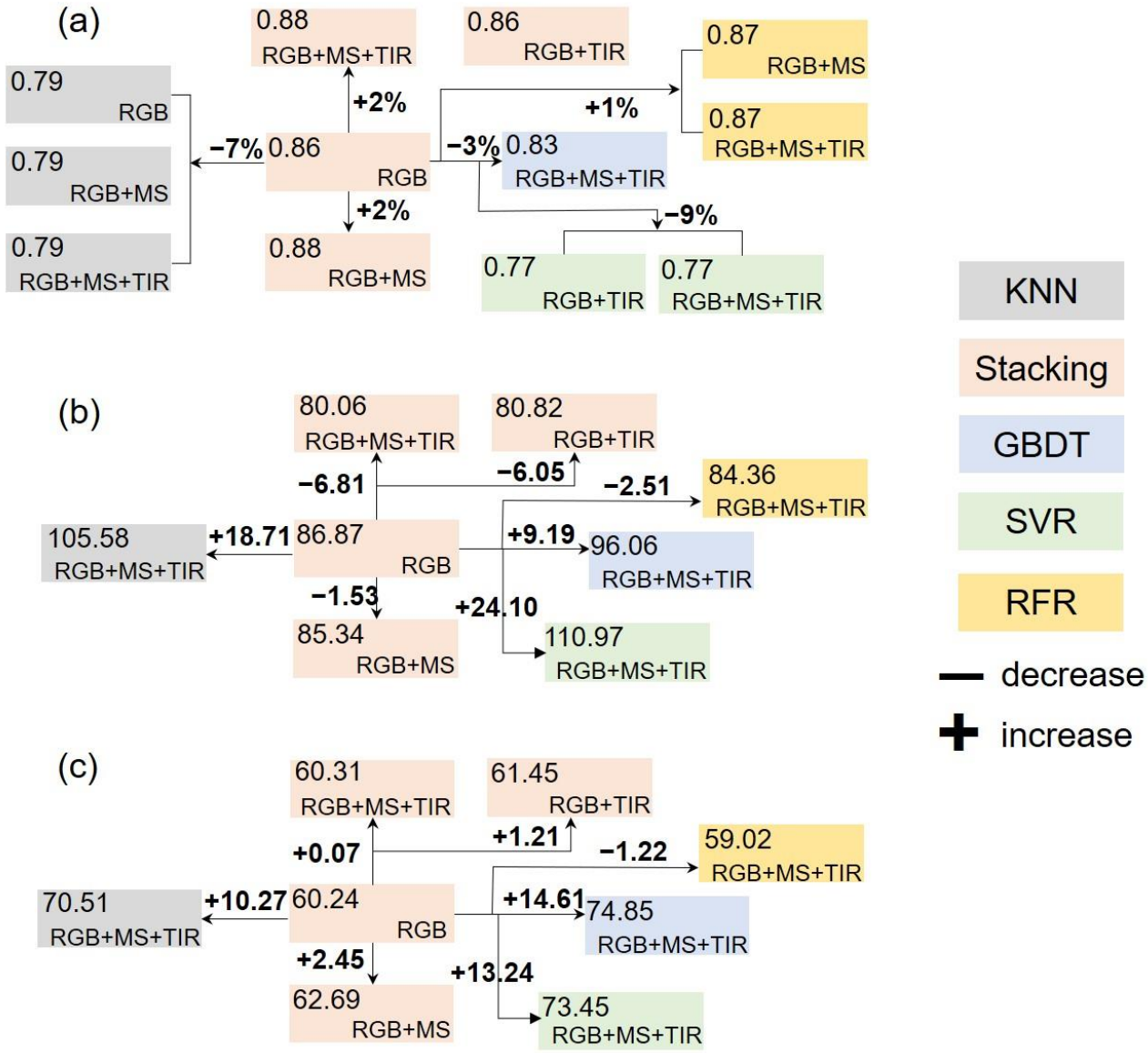

Figure 9. Comparative analysis of the estimation capability between the stacking model and other regression models. (**a**) R^2; (**b**) RMSE; (**c**) MAE.

Although the fusion of multi-source UAV imagery features has improved the estimation accuracy of alfalfa AGB, it still faced the limitations related to cost and operational feasibility in practical work. RGB sensors are preferred for crop growth monitoring due to their low cost and high spatial resolution [20,47]. Marcial-Pablo et al. [54] indicated that multispectral VIs showed better effects in the extraction of maize coverage during the aging stage. However, it was recommended to prioritize the use of RGB sensor as much as possible in practical farmland to consider the cost. Despite the rapid development in UAV remote sensing, the cost of experiment equipment remains a significant factor affecting the feasibility of monitoring in mining areas [18]. Therefore, this study proposes the following reference strategies for vegetation restoration monitoring in mining areas: (i) The stacking model integrated with multiple machine learning models offers a balance between estimation accuracy and cost considerations. The use of the stacking model combined with UAV RGB imagery features can yield better estimation of alfalfa AGB in coal waste dump. (ii) The fusion of UAV MS or TIR information with RGB features enhances the estimation accuracy of alfalfa AGB. However, we believe that employing all three sensor types is unnecessary in practical monitoring work.

5. Conclusions

Frequent spontaneous combustion activities pose a major challenge to vegetation restoration of coal waste dumps after reclamation. In response to this issue, this study explored the potential of UAV-based multi-source remote sensing data fusion (RGB, MS, and TIR) and various machine learning models for monitoring vegetation growth (alfalfa AGB) in a coal waste dump after reclamation. The key findings of this study are as follows:

(i) Fusion of UAV multi-source remote sensing data significantly improved the estimation accuracy of alfalfa AGB, although the effectiveness varied. Compared to the single RGB sensor, the estimation accuracy significantly increased when incorporating MS or TIR imagery features (R^2 increased by 0.02–0.14, RMSE and MAE decreased by 6.05–31.14 g/m^2 and 2.46–16.23 g/m^2, respectively). However, with the introduction of all three types of UAV information, the R^2 of the regression models showed no significant change, and the decrease in RMSE and MAE was less than 3 g/m^2.

(ii) The stacking model consistently outperformed RFR, GBDT, SVR, and KNN across all feature combinations, achieving accurate estimates even with limited sensor types.

(iii) The stacking model based on the RGB sensor can maintain accuracy while reducing monitoring costs. While integrating MS or TIR information further improved accuracy, it was not necessary to use all sensors for practical monitoring by mining enterprises.

(iv) A significant negative correlation between alfalfa AGB and soil temperature was observed in this study, suggesting the potential to use alfalfa AGB to guide and assess the intensity and extent of underground spontaneous combustion activities.

This study demonstrated the potential of UAVs for monitoring vegetation restoration in coal waste dumps after reclamation. Our findings provided a valuable basis for mining enterprises to develop management strategies for vegetation restoration of coal waste dumps.

Supplementary Materials: The following supporting information can be downloaded at: https://www.mdpi.com/article/10.3390/rs16050881/s1.

Author Contributions: Conceptualization, H.R. and W.X.; methodology, H.R.; software, H.R.; validation, H.R. and L.Z.; formal analysis, H.R.; investigation, H.R. and L.Z.; resources, W.X.; writing—original draft preparation, H.R.; writing—review and editing, Y.Z.; visualization, Y.Z.; supervision, W.X.; project administration, W.X.; funding acquisition, W.X. All authors have read and agreed to the published version of the manuscript.

Funding: This study received financial support from the National Natural Science Foundation of China [Grant No. 420701250].

Data Availability Statement: The data that support the findings of this study are available from the corresponding author (W.X.), upon reasonable request at present. The data are not publicly available due to data privacy.

Acknowledgments: The authors would like to thank the reviewers for their valuable comments and the editor for her help with this article.

Conflicts of Interest: The authors declare no conflicts of interest.

References

1. Xiao, W.; Zhang, W.; Ye, Y.; Lv, X.; Yang, W. Is underground coal mining causing land degradation and significantly damaging ecosystems in semi-arid areas? A study from an Ecological Capital perspective. *Land. Degrad. Dev.* **2020**, *31*, 1969–1989. [CrossRef]
2. Li, J.; Wang, J. Comprehensive utilization and environmental risks of coal gangue: A review. *J. Clean. Prod.* **2020**, *239*, 117946. [CrossRef]
3. Abramowicz, A.; Rahmonov, O.; Chybiorz, R. Environmental management and landscape transformation on self-heating coal-waste dumps in the Upper Silesian Coal Basin. *Land* **2020**, *10*, 23. [CrossRef]
4. Fabiańska, M.J.; Nádudvari, Á.; Ciesielczuk, J.; Szram, E.; Misz-Kennan, M.; Więcław, D. Organic contaminants of coal-waste dump water in the Lower-and Upper Silesian Coal Basins (Poland). *Appl. Geochem.* **2020**, *122*, 104690. [CrossRef]
5. Nádudvari, Á.; Cabała, J.; Marynowski, L.; Jabłońska, M.; Dziurowicz, M.; Malczewski, D.; Kozielska, B.; Siupka, P.; Piotrowska-Seget, Z.; Simoneit, B.R.; et al. High concentrations of HgS, MeHg and toxic gas emissions in thermally affected waste dumps from hard coal mining in Poland. *J. Hazard. Mater.* **2022**, *431*, 128542. [CrossRef]

6. Ren, H.; Zhao, Y.; Xiao, W.; Yang, X.; Ding, B.; Chen, C. Monitoring potential spontaneous combustion in a coal waste dump after reclamation through unmanned aerial vehicle RGB imagery based on alfalfa aboveground biomass. *Land. Degrad. Dev.* **2022**, *33*, 2728–2742. [CrossRef]
7. Wu, Y.; Yu, X.; Hu, S.; Shao, H.; Liao, Q.; Fan, Y. Experimental study of the effects of stacking modes on the spontaneous combustion of coal gangue. *Process. Saf. Environ.* **2019**, *123*, 39–47. [CrossRef]
8. Abramowicz, A.; Rahmonov, O.; Fabiańska, M.J.; Nádudvari, Á.; Chybiorz, R.; Michalak, M. Changes in soil chemical composition caused by self-heating of a coal-waste dump. *Land. Degrad. Dev.* **2021**, *32*, 4340–4349. [CrossRef]
9. Smoliński, A.; Dombek, V.; Pertile, E.; Drobek, L.; Gogola, K.; Żechowska, S.W.; Magdziarczyk, M. An analysis of self-ignition of mine waste dumps in terms of environmental protection in industrial areas in Poland. *Sci. Rep.* **2021**, *11*, 8851. [CrossRef]
10. Ren, H.; Zhao, Y.; Xiao, W.; Zhang, J.; Chen, C.; Ding, B.; Yang, X. Vegetation growth status as an early warning indicator for the spontaneous combustion disaster of coal waste dump after reclamation: An unmanned aerial vehicle remote sensing approach. *J. Environ. Manag.* **2022**, *317*, 115502. [CrossRef] [PubMed]
11. Ren, H.; Xiao, W.; Zhao, Y. Examining the effect of spontaneous combustion on vegetation resto-ration at coal waste dumps after reclamation: Taking *Medicago sativa* L.(alfalfa) as an indicator. *Sci. Total Environ.* **2023**, *901*, 165668. [CrossRef]
12. Ciesielczuk, J.; Czylok, A.; Fabiańska, M.J.; Misz-Kennan, M. Plant occurrence on burning coal waste–a case study from the Katowice-Wełnowiec dump, Poland. *Environ. Socio-Econ. S.* **2015**, *3*, 1–10. [CrossRef]
13. Abramowicz, A.; Rahmonov, O.; Chybiorz, R.; Ciesielczuk, J. Vegetation as an indicator of underground smoldering fire on coal-waste dumps. *Fire Saf. J.* **2021**, *121*, 103287. [CrossRef]
14. Yue, J.; Yang, G.; Li, C.; Li, Z.; Wang, Y.; Feng, H.; Xu, B. Estimation of winter wheat above-ground biomass using unmanned aerial vehicle-based snapshot hyperspectral sensor and crop height im-proved models. *Remote Sens.* **2017**, *9*, 708. [CrossRef]
15. Ge, J.; Hou, M.; Liang, T.; Feng, Q.; Meng, X.; Liu, J.; Bao, X.; Gao, H. Spatiotemporal dynamics of grassland aboveground biomass and its driving factors in North China over the past 20 years. *Sci. Total Environ.* **2022**, *826*, 154226. [CrossRef]
16. Yang, Q.; Niu, C.; Liu, X.; Feng, Y.; Ma, Q.; Wang, X.; Tang, H.; Guo, Q. Mapping high-resolution forest aboveground biomass of China using multisource remote sensing data. *GISCI. Remote Sens.* **2023**, *60*, 2203303. [CrossRef]
17. Zhang, H.; Tang, Z.; Wang, B.; Kan, H.; Sun, Y.; Qin, Y.; Meng, B.; Li, M.; Chen, J.; Lv, Y.; et al. A 250 m annual alpine grassland AGB dataset over the Qinghai–Tibet Plateau (2000–2019) in China based on in situ measurements, UAV photos, and MODIS data. *Earth. Sys. Sci. Data* **2023**, *15*, 821–846. [CrossRef]
18. Ren, H.; Zhao, Y.; Xiao, W.; Hu, Z. A review of UAV monitoring in mining areas: Current status and future perspectives. *Int. J. Coal Sci. Technol.* **2019**, *6*, 320–333. [CrossRef]
19. Bendig, J.; Yu, K.; Aasen, H.; Bolten, A.; Bennertz, S.; Broscheit, J.; Gnyp, M.L.; Bareth, G. Combining UAV-based plant height from crop surface models, visible, and near infrared vegetation indices for biomass monitoring in barley. *Int. J. Appl. Earth. Obs.* **2015**, *39*, 79–87. [CrossRef]
20. Liu, Y.; Feng, H.; Yue, J.; Jin, X.; Li, Z.; Yang, G. Estimation of potato above-ground biomass based on unmanned aerial vehicle red-green-blue images with different texture features and crop height. *Front. Plant. Sci.* **2022**, *13*, 938216. [CrossRef]
21. Zhao, Y.; Lyu, X.; Xiao, W.; Tian, S.; Zhang, J.; Hu, Z.; Fu, Y. Evaluation of the soil profile quality of subsided land in a coal mining area backfilled with river sediment based on monitoring wheat growth biomass with UAV systems. *Environ. Monit. Assess.* **2021**, *193*, 1–18. [CrossRef]
22. Fei, S.; Hassan, M.A.; Xiao, Y.; Su, X.; Chen, Z.; Cheng, Q.; Duan, F.; Chen, R.; Ma, Y. UAV-based multi-sensor data fusion and machine learning algorithm for yield prediction in wheat. *Precis. Agric.* **2023**, *24*, 187–212. [CrossRef]
23. Zhao, Y.; Zheng, W.; Xiao, W.; Zhang, S.; Lv, X.; Zhang, J. Rapid monitoring of reclaimed farmland effects in coal mining subsidence area using a multi-spectral UAV platform. *Environ. Monit. Assess.* **2020**, *192*, 1–19. [CrossRef]
24. Li, Z.; Chen, Z.; Cheng, Q.; Duan, F.; Sui, R.; Huang, X.; Xu, H. UAV-based hyperspectral and ensemble machine learning for predicting yield in winter wheat. *Agronomy* **2022**, *12*, 202. [CrossRef]
25. Maimaitijiang, M.; Sagan, V.; Sidike, P.; Hartling, S.; Esposito, F.; Fritschi, F.B. Soybean yield prediction from UAV using multimodal data fusion and deep learning. *Remote Sens. Environ.* **2020**, *237*, 111599. [CrossRef]
26. Dang, J. Problems and challenges of ecological environment in coal mine areas of Shanxi. *China Coal.* **2021**, *47*, 117–121. (In Chinese with English abstract)
27. Gitelson, A.A.; Gritz, Y.; Merzlyak, M.N. Relationships between leaf chlorophyll content and spectral reflectance and algorithms for non-destructive chlorophyll assessment in higher plant leaves. *J. Plant. Physiol.* **2003**, *160*, 271–282. [CrossRef]
28. Kataoka, T.; Kaneko, T.; Okamoto, H.; Hata, S. Crop growth estimation system using machine vision. In Proceedings of the 2003 IEEE/ASME International Conference on Advanced Intelligent Mechatronics, Kobe, Japan, 20–24 July 2003; Volume 2, pp. 1079–1083.
29. Woebbecke, D.M.; Meyer, G.E.; Von Bargen, K.; Mortensen, D.A. Color indices for weed identification under various soil, residue, and lighting conditions. *Transact. ASABE* **1995**, *38*, 259–269. [CrossRef]
30. Neto, J.C. *A Combined Statistical-Soft Computing Approach for Classification and Mapping Weed Species in Minimum-Tillage Systems*; The University of Nebraska-Lincoln: Lincoln, NE, USA, 2004.
31. Louhaichi, M.; Borman, M.M.; Johnson, D.E. Spatially located platform and aerial photography for documentation of grazing impacts on wheat. *Geocarto. Int.* **2001**, *16*, 65–70. [CrossRef]

32. Chianucci, F.; Disperati, L.; Guzzi, D.; Bianchini, D.; Nardino, V.; Lastri, C.; Rindinella, A.; Corona, P. Estimation of canopy attributes in beech forests using true colour digital images from a small fixed-wing UAV. *Int. J. Appl. Earth Obs.* **2016**, *47*, 60–68. [CrossRef]
33. Gitelson, A.A.; Kaufman, Y.J.; Merzlyak, M.N. Use of a green channel in remote sensing of global vegetation from EOS-MODIS. *Remote Sens. Environ.* **1996**, *58*, 289–298. [CrossRef]
34. Rouse, J.W.; Haas, R.H.; Schell, J.A.; Deering, D.W. Monitoring vegetation systems in the Great Plains with ERTS. *NASA Spec. Publ.* **1974**, *351*, 309.
35. Gong, P.; Pu, R.; Biging, G.S.; Larrieu, M.R. Estimation of forest leaf area index using vegetation indices derived from Hyperion hyperspectral data. *IEEE. Trans. Geosci. Remote* **2003**, *41*, 1355–1362. [CrossRef]
36. Huete, A.; Didan, K.; Miura, T.; Rodriguez, E.P.; Gao, X.; Ferreira, L.G. Overview of the radiometric and biophysical performance of the MODIS vegetation indices. *Remote Sens. Environ.* **2002**, *83*, 195–213. [CrossRef]
37. Pearson, R.L.; Miller, L.D. Remote mapping of standing crop biomass for estimation of the productivity of the shortgrass prairie. *Remote Sens. Environ.* **1972**, *VIII*, 1355.
38. Rondeaux, G.; Steven, M.; Baret, F. Optimization of soil-adjusted vegetation indices. *Remote Sens. Environ.* **1996**, *55*, 95–107. [CrossRef]
39. Chen, J.M. Evaluation of vegetation indices and a modified simple ratio for boreal applications. *Can. J. Remote Sens.* **1996**, *22*, 229–242. [CrossRef]
40. Barnes, E.M.; Clarke, T.R.; Richards, S.E.; Colaizzi, P.D.; Haberland, J.; Kostrzewski, M.; Waller, P.; Choi, C.; Riley, E.; Thompson, T.; et al. Coincident detection of crop water stress, nitrogen status and canopy density using ground based multispectral data. In Proceedings of the Fifth International Conference on Precision Agriculture, Bloomington, MN, USA, 16 July 2000; Volume 1619, p. 6.
41. Haralick, R.M.; Shanmugam, K.; Dinstein, I.H. Textural features for image classification. *IEEE.T. Syst. Man. Cy-s.* **1973**, *6*, 610–621. [CrossRef]
42. Jackson, R.D.; Reginato, R.J.; Idso, S. Wheat canopy temperature: A practical tool for evaluating water requirements. *Water. Resource Res.* **1977**, *13*, 651–656. [CrossRef]
43. Idso, S.B.; Jackson, R.D.; Pinter, P.J., Jr.; Reginato, R.J.; Hatfield, J.L. Normalizing the stress-degree-day parameter for environmental variability. *Agric. Meteorol.* **1981**, *24*, 45–55. [CrossRef]
44. Kursa, M.B.; Rudnicki, W.R. Feature selection with the Boruta package. *J. Stat. Softw.* **2010**, *36*, 1–13. [CrossRef]
45. Shu, M.; Zuo, J.; Shen, M.; Yin, P.; Wang, M.; Yang, X.; Tang, J.; Li, B.; Ma, Y. Improving the estimation accuracy of SPAD values for maize leaves by removing UAV hyperspectral image backgrounds. *Int. J. Remote Sens.* **2021**, *42*, 5862–5881. [CrossRef]
46. Wolpert, D.H. Stacked generalization. *Neural Netw.* **1992**, *5*, 241–259. [CrossRef]
47. Zhai, W.; Li, C.; Cheng, Q.; Mao, B.; Li, Z.; Li, Y.; Ding, F.; Qin, S.; Fei, S.; Chen, Z. Enhancing Wheat Above-Ground Biomass Estimation Using UAV RGB Images and Machine Learning: Multi-Feature Combinations, Flight Height, and Algorithm Implications. *Remote Sens.* **2023**, *15*, 3653. [CrossRef]
48. Liang, Y.; Kou, W.; Lai, H.; Wang, J.; Wang, Q.; Xu, W.; Wang, H.; Lu, N. Improved estimation of aboveground biomass in rubber plantations by fusing spectral and textural information from UAV-based RGB imagery. *Ecol. Indic.* **2022**, *142*, 109286. [CrossRef]
49. Li, W.; Niu, Z.; Chen, H.; Li, D.; Wu, M.; Zhao, W. Remote estimation of canopy height and aboveground biomass of maize using high-resolution stereo images from a low-cost unmanned aerial vehicle system. *Ecol. Indic.* **2016**, *67*, 637–648. [CrossRef]
50. Wu, S.; Deng, L.; Guo, L.; Wu, Y. Wheat leaf area index prediction using data fusion based on high-resolution unmanned aerial vehicle imagery. *Plant Methods* **2022**, *18*, 68. [CrossRef]
51. Wang, Q.; Che, Y.; Shao, K.; Zhu, J.; Wang, R.; Sui, Y.; Guo, Y.; Li, B.; Meng, L.; Ma, Y. Estimation of sugar content in sugar beet root based on UAV multi-sensor data. *Comput. Electron. Agr.* **2022**, *203*, 107433. [CrossRef]
52. Maimaitijiang, M.; Ghulam, A.; Sidike, P.; Hartling, S.; Maimaitiyiming, M.; Peterson, K.; Shavers, E.; Fishman, J.; Peterson, J.; Kadam, S.; et al. Unmanned Aerial System (UAS)-based phenotyping of soybean using multi-sensor data fusion and extreme learning machine. *ISPRS. J. Photogramm.* **2017**, *134*, 43–58. [CrossRef]
53. Feng, L.; Zhang, Z.; Ma, Y.; Du, Q.; Williams, P.; Drewry, J.; Luck, B. Alfalfa yield prediction using UAV-based hyperspectral imagery and ensemble learning. *Remote Sens.* **2020**, *12*, 2028. [CrossRef]
54. Marcial-Pablo, M.D.J.; Gonzalez-Sanchez, A.; Jimenez-Jimenez, S.I.; Ontiveros-Capurata, R.E.; Ojeda-Bustamante, W. Estimation of vegetation fraction using RGB and multispectral images from UAV. *Int. J. Remote Sens.* **2019**, *40*, 420–438. [CrossRef]